Detergent Foam Images as Analogue/Digital Model Fluids. 1. Phase Behavior and Effective Pair Potentials

Daniel J. Graham,* Peter Magdalinos,† and Dante Pimentel

Department of Chemistry, Loyola University of Chicago, Chicago, Illinois 60626

Received: December 9, 1996; In Final Form: July 9, 1997[⊗]

Detergent foam images are investigated as analogue/digital (A/D) models for simple fluids. Results of foam preparation/image processing experiments with quasi-two-dimensional systems are illustrated. In the analysis, the pair and triplet correlation functions, $g(r)$ and $\xi(\Theta,s;r)$, are measured for the vertexes of plateau border networks. The phase morphology is characterized by the amplitude and extent of oscillations in $g(r)$. Effective pair potentials $u(r)$ are calculated via the lowest order equation in the Born−Yvon−Green hierarchy. The $u(r)$ are further investigated via Monte Carlo calculations and the Morse function. The experimental data are used to calculate the pair correlation entropy and the compressibility factor as functions of particle number density. These and other observables enable comparisons between the model systems and real atomic fluids. Overall, the results show foam images to mimic fluid structure at the atomic level in several respects. For the experimental conditions discussed, successions of images offer novel views of liquid → gas transitions.

I. Introduction

In 1948, Bragg and Nye described experiments with free-floating soap bubble rafts.[1] These systems attracted attention due to their imitation of atom-packing behavior in crystals. Bragg and Nye's results were recorded photographically and offered the first simulations of crystal growth and defect migration at the "atomic scale". In the experiments, the particle numbers approached 10^5, depending on the sample preparation details. Digital computers of that era fell orders of magnitude short in handling model populations of this size.[2]

Other researchers took the idea several steps further. For example, Dyson related the visible light diffraction properties of closest packed soap bubbles to X-ray diffraction by atomic systems.[3] Using soap bubble rafts, Fukishima and Ookawa studied lattice vibration and shear stress effects on crystallization.[4] Smith used detergent foams as models for amorphous metals, drawing on the parallels between fused gas bubbles and metallic grains.[5] Bernal related molecular packing statistics of the liquid phase to the irregular polytope structures in foams. A variety of mechanical constructions were inspired on this basis in the first geometrical studies of liquid structure.[6] While all these approaches were supplanted eventually by computer simulations (Monte Carlo and molecular dynamics), all of them are time-honored for the *analogue* views they provided. What nature obscures at the atomic scale was revealed in part by simple laboratory experiments.

Foams and their model applications have resurged as subjects in the current literature. For example, the experiments by Stavans and Glazier have provided xerographic tests of von Neumann's law and other fundamentals of cellular patterns.[7] Theories by a number of researchers have established the physics of foam morphology and coarsening kinetics.[8] As things stand today, foams serve as models for biological cells, metallic grains, and magnetic bubbles, among other systems famous for their complexity. Several reviews are available, particularly concerning topology and dynamics in two dimensions (2D).[9] A sampling of most recent works shows research to continue internationally along these lines.[10] Note also that foam structures have been investigated in fatty acid monolayers using fluorescence microscopy.[11] Independent reviews by Mohwald, McConnell, and Knobler include perspectives on this subject.[12−14]

Detergent foams are the subject of the present study, the focus shifted to problems of fluid structure. Specifically, the intersections of gas bubble walls in disordered samples are viewed as atoms of a monodisperse fluid. Snapshots of quasi-2D systems are bridged with several conceptuals tailored for liquids and gases. The link is forged via simple benchtop experiments and computer image processing.

The motivation is as follows. For the past several years, this lab has investigated the behavior of fluids and glasses under a variety of conditions.[15] The experiments have been almost all spectroscopic, and the systems have invariably entailed organic aromatic molecules. Yet endeavor has included a search for models (some off the beaten trail) which offer *both* benchtop access and particlewise information. The attractive idea was to model fluids in a way alternative to computer simulations of present day. As things turned out, research both contemporary and of yesteryear provided the sought-after model, with the assistance of digital image processing. In the studies which transpired, all the data are analogue/digital (A/D) in substance, deriving from the images of wet samples packaged on a lab benchtop.

A portion of our results is reported in this and the companion paper. The first establishes the essentials by which foam images serve as model fluids. Sample results are illustrated, and the phase and potential properties are characterized. In the work which follows, attention turns to the neighborship partition of the radial distribution function.[16] This offers first comparisons between the model fluid data and select theory by previous researchers, with applications to real atomic systems. In a forthcoming report, successions of foam images reveal the symmetry rules involved in the transit between crystal and liquid morphologies.[17]

II. Detergent Foams and Atomic Fluids: Analogies and Distinctions

The top panel of Figure 1 shows the shadow projection of a quasi-2D detergent foam: water plus surfactant plus gas trapped

* To whom correspondence should be addressed. Fax (773) 508-3086; E-mail DGRAHA1@LUC.EDU.

† Present address: Department of Chemistry, Northern Illinois University, DeKalb, IL, 60115.

⊗ Abstract published in *Advance ACS Abstracts,* December 1, 1997.

S1089-5647(96)04029-1 CCC: $14.00

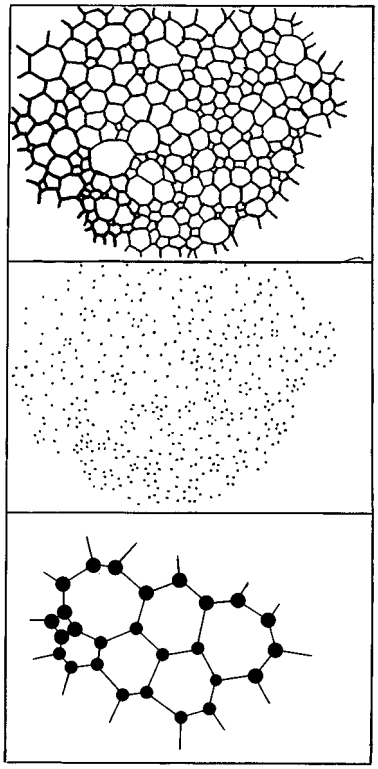

Figure 1. Detergent foam, vertex positions, and icons. Top panel shows a portion of a 2D detergent foam composed of plateau borders (darkened regions) and trapped air (clear regions). The borders occlude view of parallel ones which wet the opposite container plate. The middle frame depicts the center-of-mass positions of the connect-three vertexes. The bottom frame contains icons used to represent atoms and chemical bonds. The pattern was inscribed using a small portion of the top panel network as a template.

between parallel plexiglass plates. The blackened areas correspond to the aqueous solution which composes the plateau borders,[18] while the clear areas represent the gas regions. The middle panel marks the center-of-mass positions of the connect-three vertexes. The bottom panel shows results of using a small portion of sample as a template. Via this template, *icons* for atoms and chemical bonds have been inscribed.[19]

By Figure 1, several analogies between detergent foams and atomic fluids are apparent. A foam is an assembly of three types of building blocks: vertexes, interconnecting walls, and trapped gas. In an analogous fashion, a fluid (liquid or dense vapor) is composed of atoms, chemical bonds, and free volume. A shadow pattern such as in Figure 1 is disordered on extended length scales, yet (as will be shown) demonstrates some amount of short-range order. Similarly, fluids express a shell structure about any given atom, yet are lacking in correlations beyond a certain distance.[20] The shapes of both fluids and detergent foams are strongly influenced by their containers.

Other analogies can be cited, yet it is more important to note a few distinctions. One is that a real fluid is generally at equilibrium, given conditions of fixed temperature, pressure, and number of particles. As such, the structure and thermodynamics are independent of history; the conditions are always restored if displaced momentarily from equilibrium. By contrast, a detergent foam has a structure which is time-dependent and only mildly restorative in nature. This is on account of gas and liquid diffusion from high-curvature sources to low-curvature sinks (liquid drainage is a factor in 3D samples). The transport effects all include the loss of vertexes and walls over time.

A second distinction is topology. Atoms in a real fluid are subject to forces in 3D, while the coordination number is variable from site to site. Shadow patterns such as in Figure 1 are obviously different given their 2D quality. Moreover, the connect-three-ness of plateau borders offers a topological order not present in real fluids.

A third distinction concerns uniqueness of structure. For a real fluid, scattering data such as X-ray must be interpreted entirely in terms of atom pair correlations: the structure factor by itself provides no direct information about higher order correlations.[21] This poses serious knowledge gaps about how atoms are arranged in a real fluid. Inevitably, multiple structures are equally consistent with a given set of diffraction data. A foam sample is different, given a structure which (especially in 2D) can be measured unambiguously by direct-space imaging. Thus, a foam image and its homologously constructed icon map afford particlewise information much like that realized in computer simulations of fluids.

The analogies between foams and fluids are those which can be drawn between liquid-plus-trapped gas and electric charges-plus-free volume. Yet the distinctions impose certain conditions on foam image data and their interpretation. Thus, because of the first distinction (time dependence), attention will be confined to samples which evolve "slowly" over time. For these quasi-static cases, a sample at any given instant will be regarded in a type of pseudoequilibrium state, having accessed all of the "fast" degrees of freedom. This will be a key assumption when applying thermodynamics and statistical mechanics (equilibrium ideas). Several of the referenced works on foam coarsening offer valuable discussion on this point.[7,8] The time-dependent nature of detergent foams turns out to be not without experimental advantage. This is because a succession of model fluids can be realized from one initial sample preparation.

By the second distinction (topological order and dimensionality), the word "fluid" must obviously be used in a very general sense. "Glass" may be a more appropriate term, much in the same spirit as Bernal's work and other mechanical studies of liquids.[6,22] Yet by the third distinction (uniqueness of structure), one finds much of the lure for pursuing foam imaging experiments in the first place. Indeed, for particle configurations such as in Figure 1, the phase characteristics and effective pair potentials can be established rather precisely. Entities such as these are central to fluid research and are therefore the major objectives of this paper. The next section outlines the strategy by which they emerge.

III. Detergent Foams and Atomic Fluids: Analytical Strategy

In both model and real fluids, particle placement statistics tie all the small length scale properties to the large-scale ones. The connections are made by the particle correlations (single, pair, etc.) and the potential functions. The pair correlation function $g(r)$ is defined for this work as follows:

$\rho g(r) =$ average density of plateau border vertexes (model atom in the icon map) at distance r given that a tagged or reference particle lies at the origin (1)

where

$2\pi\rho r g(r)\,\mathrm{d}r =$ average number of particles at distance between r and $(r + \mathrm{d}r)$ (2)

and

$$\int 2\pi\rho r g(r)\,\mathrm{d}r = N - 1 \qquad (3)$$

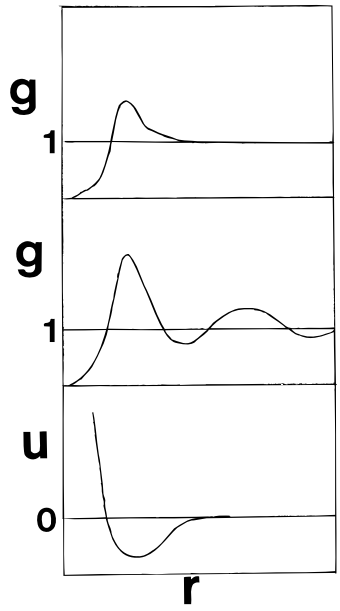

Figure 2. Generic pair distribution and potential functions. Top and middle panels illustrate $g(r)$ for generic gas and liquid states, respectively. In both panels, $g(r) = 1$ for an ideal gas has been included as a reference. The bottom panel illustrates generic $u(r)$ companion with $g(r)$. The case for an ideal gas, namely $u(r) = 0$, has been included.

In the above, ρ is the number density equivalent to N/A, the total number of particles in a sample divided by the total area. Position r is asserted as the independent variable, although the dependence on temperature and pressure is understood. Physically speaking, $g(r)N/A$ measures the likelihood of finding a neighboring particle on a circle of radius r inscribed about a randomly chosen particle.

As is well-known, $g(r)$ for an atomic fluid is readily interpreted alongside a pair potential $u(r)$.[20] For example, in Figure 2 (top and middle panels) $g(r)$ equals zero at small r; this is consistent with the strong repulsive forces operating via generic $u(r)$ (bottom panel). The oscillations in $g(r)$ delineate the shell structure about the reference particle, with the first maximum corresponding more or less to the potential minimum. The oscillations are more prominent in the cases of lower temperature and/or higher particle density, such as in the middle frame. In this way, distinct signatures for gas and liquid states (top and middle panels, respectively) are provided by $g(r)$. Of course, the trivial case is when $u(r) = 0$. In this "perfect gas" case, $g(r) = 1$ where correlations are absent on all length scales. By contrast, $g(r) = 1$ for an interacting fluid ($u(r) \neq 0$) only where r exceeds the pair correlation length.

For a real fluid, $g(r)$ follows from the structure factor measured by X-ray or neutron scattering.[21] In turn, quantities such as the free energy and pressure can be related to integral functions involving both $g(r)$ and $u(r)$.[20−21,23] However, measurement of $g(r)$ by itself does not render unique $u(r)$, except in the limit of zero density. Arriving at pair potentials more typically entails a mix of experiment and modeling, for example molecular beam spectroscopy and Monte Carlo calculations.[24,25] The situation is quite different when viewing detergent foams as model fluids. As will be shown, one can arrive at *both* the pair distribution and potential functions, irrespective of particle number density. These are the luxuries of direct-space imaging not afforded in X-ray and neutron diffraction.

The application of integral equations to fluid structure problems has a distinguished history, one landmark being the Born−Yvon−Green (BYG) hierarchy.[26] Throughout this project, it was the lowest order in this hierarchy of equations, which

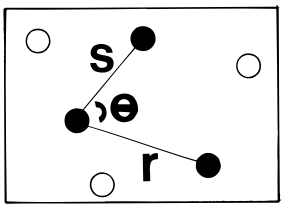

Figure 3. Geometry used in computing the triplet distribution function $\xi(\Theta,s;r)$. The correlated particles are indicated by blackening.

was used to arrive at $u(r)$. In so doing, a strategy originated by Braun and Owicki for membrane protein distributions was followed.[27] The lowest order BYG equation is defined for our experiments as follows:

$$k_B T\,(\mathrm{d}/\mathrm{d}r)\ln g(r) = f(r) + \int_0^\infty \int_0^{2\pi} f(s)\,\xi(\Theta,s;r)\cos\Theta\,\mathrm{d}\Theta\,\mathrm{d}s \quad (4)$$

where the lhs is a mean force and $k_B T$ has its usual meaning. The rhs terms include the pair force $f(r) = -\mathrm{d}u(r)/\mathrm{d}r$ which is subject to the neighbor effects contained in the integral. In the integrand, $\xi(\Theta,s;r)$ is the triplet correlation function which measures the probability of finding a particle at polar coordinates Θ,s, given a pair separated by r. Figure 3 shows the particular geometry used in evaluating $\xi(\Theta,s;r)$. This is basically the same geometry used in Braun and Owicki's analysis, although the notation has been altered here slightly to avoid possible confusion (the triplet function was designated ρ in their work). Note that in eq 4 the integrand is weighted by the projection of the pair force on the imaginary line separating pair-correlated particles (cf. Figure 3).

It should be emphasized that eq 4 marks only one approach to fluid structure; others would include the Percus−Yevick and hypernetted chain equations.[28] While this paper is not the venue to discuss the merits of one integral equation versus another, BYG was chosen for its tractability and transparency. For the authors, there was great appeal in sidestepping approximations normally made in evaluating triplet correlations. In this work, both $g(r)$ and $\xi(\Theta,s;r)$ (and ultimately $u(r)$) follow directly from the icon maps constructed for each foam sample. The maps and foam samples themselves provide the respective digital and analogue components of the model fluids.

IV. Experimental Section

A variety of foaming methods, sample conditions, and methods of analysis were explored over the course of this project. As is familiar on a daily basis, foams are prepared by forcing gas through a mixture of water and detergent. For the initial survey experiments, household products such as dishwashing liquids and shampoos were used as the sample materials. Quasi-2D systems were prepared simply by sandwiching freshly prepared foam (aqueous solution plus trapped air) between the reversed plates of standard (12 cm diameter) Petri dishes. The plateau border networks were projected as shadow images onto large sheets (5500 cm^2) of graph paper, using an overhead projector. This enabled portions of vertex constellations to be hand-traced and tabulated in real time, however tediously. Later imaging experiments incorporated snapshot photography; the resulting Kodachrome slides were then reprojected for extensive hand-tracing and vertex tabulation. While effort must be made to avoid the errors due to parallax, these procedures proved quite effective during the survey stages of research. For example, they allowed for a spatial resolution of approximately 0.02 mm and accommodated vertex populations as high as about 2000.

Several necessary refinements were developed in the later stages. First, for consistency, attention was confined to closed, binary solutions (water plus purified surfactant compound) at controlled temperature. The most extensive database was established for samples composed of distilled water and sodium dodecyl sulfate (SDS, Biorad electrophoresis grade). Air or pure nitrogen was used as the gas, while the plateau borders were supported by epoxy-sealed plexiglass plates (24×30 cm^2) separated by fixed O-rings (0.5 cm diameter). With practice, it became feasible to prepare foam samples "reproducibly" at a given surfactant concentration (usually ca. 0.1 M) by controlled gas injection using an adjustable capillary nozzle. Also with practice, a uniform agitation procedure yielded consistent and comparable results. By "reproducibly", one means that control could be exerted on the vertex number density and placement statistics as ascertained by $g(r)$ and other topological measurements. In these later experiments and analysis, an optical scanner (HP Deskscan II) and desktop computer proved indispensable in capturing the foam morphology in a digital (Windows 3.0 bitmap) format. By this approach, 200 kbytes was the typical raw image file size. In establishing the icon maps, $g(r)$, and $\xi(\Theta,s;r)$, it was most expedient to discriminate the vertexes as the pixel clusters forming the intersection of three bonds. In so doing, Gaussian functions were assigned by computer software and centered at each cluster center-of-mass. The width of each function was usually made equivalent throughout the plateau border network. In this way, a "monodisperse" fluid was established for each vertex constellation represented in a bitmap file. Each model fluid was composed of 6000−10 000 virtual particles, depending on the initial foaming conditions and the stage of evolution. The Gaussian functions were intended to mimic (more or less) the electric charge distribution in atoms. While this choice of functions is arbitrary, the results do not change substantially if other simple constructs (e.g. first-order exponentials with comparable decay length) are used.

In computing $g(r)$, each ith particle of an icon map was tagged as a reference particle, while the $j \neq i$ particles falling within a ring of radius r and width Δr were integrated to give a quantity $\sum_i$. In so doing, r approximated the distance separating the i,j particles, while Δr approximated half of the particle Gaussian width. The quantity $g_i(r)$ was then computed as $\sum_i A/(2\pi\Delta r N_v)$, in accordance with eq 2. Final $g(r)$ was established by averaging the $g_i(r)$ over an entire particle constellation. A similar approach was taken in acquiring $\xi(\Theta,s;r)$, although demanded considerably more in terms of computer hard drive storage, random access memory, and processing time. In the $\xi(\Theta,s;r)$ computations, each bitmap file was subdivided into equal-sized bins (12−14 typical) for averaging purposes. Significantly, there were no major differences between the results derived from many of the survey (hand-tabulation) and later stage (digital scanner) efforts.

Equation 4 was solved by successive approximation using a least-squares algorithm; in each case, several trajectories around the pair-force kernel were explored. Pair correlation functions were also computed using the potentials obtained via eq 4, at particle densities which approximated the experimental conditions. Here a Monte Carlo (MC) routine written by the authors was used to establish the configurations allied with the minimum potential energy. Note that in applying eq 4 and MC calculations, $k_B T$ was taken as fixed by the equilibrium thermodynamic temperature, with (in the interest of simplicity) no appeal to alternative quantities, e.g. a fictive temperature dependent on foam structure. By such an approach, all structure characteristics were expressed in $u(r)$, $g(r)$, and other thermodynamic quantities.

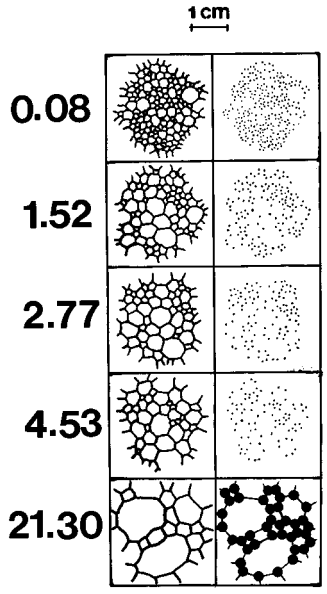

Figure 4. Portion of quasi-2D detergent foam at different evolutionary stages. The lhs panels illustrate the plateau border networks, while rhs panels mark center-of-mass positions of the vertexes. The time following the initial sample preparation is noted in hours alongside each frame pair. The atom and chemical bond icons inscribed by computer software are depicted in the bottom rhs panel. The particle diameters correspond to the width of each assigned Gaussian function. The length scale is indicated at the top of the illustration.

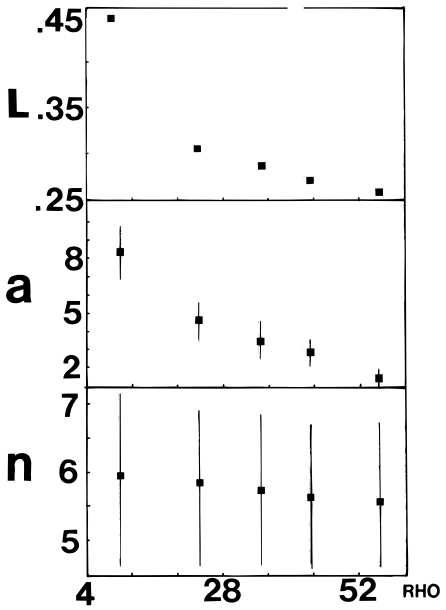

Figure 5. Topological observables of foam images. Horizontal scale indicates the vertex number density in units of vertexes/cm^2. The average number of sides n and area A per gas bubble are plotted in the bottom and middle panels, respectively. Vertical bars mark the average ± one standard deviation. The top panel plots the dimensionless quantity L defined in the text.

486DX and Pentium PCs (Compaq 50 MHz and Gateway 120 MHz, respectively) were used in all of the calculations.

For conciseness, results allied with one sample preparation are illustrated and discussed. The data in Figures 4−10 originate from a quasi-2D foam sample of area 516 cm^2 composed of distilled water, SDS (8.03×10^{-2} M), and air near atmospheric pressure. The gap between the supporting plexiglass plates was 1.6 mm, while the temperature was maintained at 294 K. The initial number density was ca. 58 vertexes/model particles per cm^2. The conditions were "disordered" in the sense that except for the connect-three-ness of plateau vertexes, extended

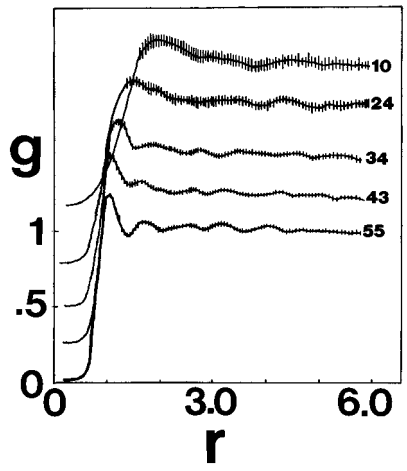

Figure 6. Pair correlation data. Numbers along the horizontal axis refer to distance in millimeters. Individual $g(r)$ are displaced by 0.25 for clarity. Vertical hatch marks indicate the average ± one standard deviation. The number densities (particles/cm^2) are indicated for each plot.

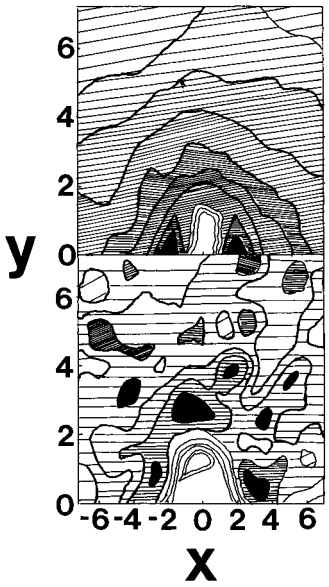

Figure 7. Pair correlation density maps. Numbers along the horizontal and vertical axes refer to distance in millimeters. The degree of blackness is proportional to the probability of finding a neighbor particle in relation to the reference particle at the origin. Upper and lower panels correspond to the ρ values of 56 and 10 particles/cm^2.

symmetry and long-range order were not at all apparent in the initial and developing stages. The samples were closed systems such that fluid and gas amounts were conserved at all times. Thus, gas pressure gradients and interfacial energy in the plateau borders were the sources of irreversibility. The essentials of phase behavior and pair potentials are embodied in these data.

V. Results

Figure 4 illustrates one neighborhood of a quasi-2D foam sample at several stages of evolution. All of the images are presented at the same level of magnification, and the length scale has been marked at the top of the figure. The frame pairs display the plateau border structure (lhs) along with the center-of-mass configurations of the connect-three vertexes (rhs). The times following the sample preparation are noted in hours alongside each frame pair, although these (and foam kinetics in general) will be incidental to the discussion. The bottom

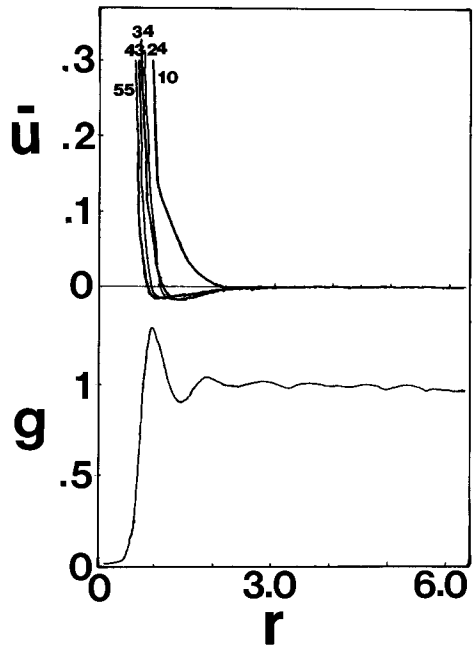

Figure 8. Top panel: Effective pair potentials $u(r)/k$BT. Number densities are indicated for each plot. Numbers along the horizontal axis refer to distance in millimeters. Bottom panel: $g(r)$ computed from Monte Carlo calculation. For the illustrated case, the particle density and potential conditions coincide with the lowermost $u(r)/k_BT$ graph in the upper panel.

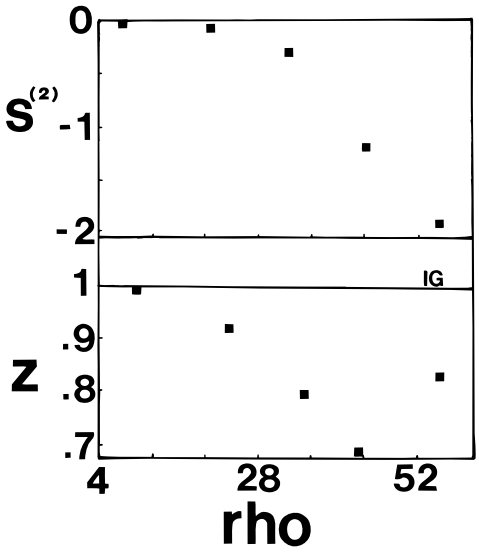

Figure 9. Compressibility factor and pair correlation entropy. The horizontal scale indicates number density in units of particles/cm^2. Top and bottom panels plot $S^{(2)}$ and Z as defined in text.

rhs panel includes the icon pattern inscribed for this neighborhood of the bitmap file. Note that the curvature and size variability of the plateau borders are washed away when transposing an image into an icon map. Further, there is inevitable overlap between neighboring model particles. Since a Gaussian function is affiliated with each particle, the fluid model does not conform strictly to hard disk physics.

The general traits of foam evolution (coarsening) are apparent in Figure 4. One sees that the vertex population and total bond length diminishes over time so as to minimize the interfacial free energy. The average gas bubble area grows, with the larger bubbles gradually consuming the smaller ones. A detailed discussion of this process is given in several of the referenced works, for example in connection with Stavans and Glazier's experiments.[7]

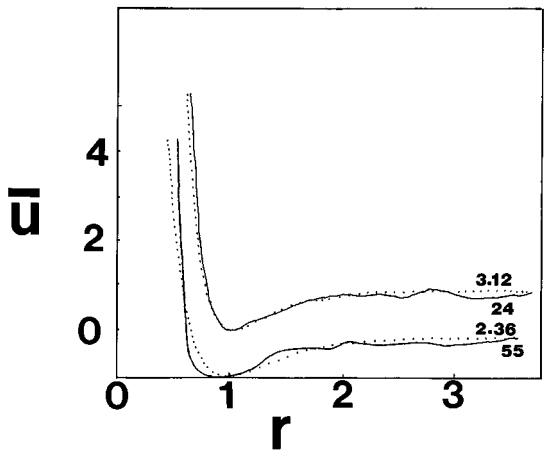

Figure 10. Rescaled u (solid lines) and best-fit Morse replicas (dotted). For each case, the minimum value $= -1$ at $r = 1$. Plots are labeled by ζ and ρ values.

Figure 5 quantifies three topological observables in the image data. The top frame plots quantity L, defined as the standard deviation of nearest neighbor particle distance divided by the average. The middle and lower frames illustrate the average bubble area (a, mm^2 units) and average number of gas bubble sides (n). All of these quantities are presented as functions of number density ρ measured in particles/cm^2. The vertical bars in the lower two frames denote the average $\pm$ one standard deviation. Note that the more significant changes concern L and average a; changes in a and n involve both the average and deviation. For later stage foam samples, the second moment values of n fall in the range of 1.4−1.7. Such are consistent with scaling values reported by Stavans and Glazier.[7]

Figures 4 and 5 convey the basics of foam coarsening, yet may offer few clues about model fluid structure. Figure 6 addresses this matter by showing $g(r)$ for each icon map, of which Figure 4 registers only small neighborhoods. The solid lines denote the average, while the vertical bars indicate the average $\pm$ one standard deviation. The graphs are labeled by the allied ρ values and are displaced by 0.25 for clarity. Not surprisingly, the rise in $g(r)$ occurs at approximately the nearest neighbor separation length. For samples having $\rho > 30$ particles/cm^2 ($L < 0.29$), the correlation range measured by experimentally significant oscillations extends several of these unit lengths. By contrast, the $g(r)$ plots allied with $\rho \approx 24$ and 10 particles/cm^2 are quite diffuse. The former of these two demonstrates a very slight peak at $r \approx 4.3$ mm. Only a single broad peak at $r \approx 2.1$ mm is experimentally significant in the other, as the oscillation amplitude at higher r rivals the standard deviations.

It is straightforward to compute

$$N_D = \int_0^{r_D} 2\pi r \rho g(r)\, dr \qquad (5)$$

by numerical integration. By taking r_D to be the first minimum in $g(r)$, one obtains N_D values of about 3.2 for samples with $\rho > 30$ particles/cm^2. It is of further interest to view pair correlation data as density plots analogous to Patterson diagrams in the crystallography literature.[29] In Figure 7, sample plots are illustrated for two of the cases under consideration. The horizontal and vertical axes denote the distance in millimeters from the reference particle centered at the origin. The degree of blackness is proportional to the probability of locating a neighboring particle relative to the origin. Note how the sample with higher particle number density (upper panel) manifests a series of irregular bands. By contrast, the plot recorded at lower ρ (lower panel) asserts multiple islands and peninsulas.

The upper panel of Figure 8 illustrates $\bar{u} = u(r)/k_BT$ for the samples (again labeled by ρ values) which were derived from experimental $g(r)$, $\xi(\Theta,s;r)$, and eq 4. The abscissa is marked in millimeter units using the same scale as in Figure 6. One sees that in all cases a "wall" appears at low r in the $\bar{u}$ functionality. The wall position approximates the nearest neighbor separation length, as with the rise of $g(r)$. The wall is pushed outward as the particle number density decreases. For the experimental run illustrated, a shallow well is most evident for the higher density samples ($\rho > 30$ particles/cm^2). This well extends more than three nearest neighbor separation lengths in the highest density sample and ca. 1.5 lengths for the lower density samples. The well is of near-zero depth for the lowest density sample.

The $g(r)$ and $\bar{u}$ thus illustrated derive from A/D model data. By the same token, u can be used to regenerate $g(r)$ in a process which is solely digital. For example, the bottom panel of Figure 8 plots $g(r)$ obtained using the pair potential allied with $\rho \approx 56$ particles/cm^2 via a Monte Carlo method. The calculation was carried out at such a particle density so as to locate the configuration of lowest energy. The $g(r)$ of this illustration was computed on the basis of this configuration. In the calculation, the particles were taken to be disklike, with widths/densities specified by Gaussian functions.

Figure 9 illustrates two (out of many possible) thermodynamic quantities which can follow from the correlation data: the compressibility factor $Z = p/\rho k_BT$ and the pair correlation entropy

$$S^{(2)} = -(1/2)\rho \int dr\, g(r) \ln g(r) \qquad (6)$$

as functions of ρ. The Z values were obtained by averaging the pair force between all the particles separated by an imaginary interface of unit length. The procedure used followed one described by Hill in his textbook discussion of classical fluids.[23] The pair correlation entropy was computed using experimental $g(r)$ in accordance with theoretical work by Wallace.[30]

The upper panel of Figure 10 contains two of the $\bar{u}$ functions (solid lines) which have been rescaled so that the minimum value $= -1$ at $r = 1$. This figure also illustrates the best-fit replicas (dotted lines) devised according to the Morse potential

$$\bar{u} = \exp[\zeta(1-r)]\{\exp[\zeta(1-r)] - 2\} \qquad (7)$$

In modeling data via eq 7, a single parameter ζ characterizes the potential shape. The range of the attractive part decreases with increasing ζ, while the wall is "hardened" at the same time. In Figure 10, the best-fit values of ζ are listed alongside each rescaled u and replica along with the number density values. The Morse replicas of u derived from detergent foam data always have ζ values in the range 2−4.

VI. Discussion

Detergent foams are mixtures of liquid and gas stabilized by surface active molecules. Their commercial applications are numerous and parallel those of oil−water emulsions.[31] As sketched in section I, foams also serve as models for a variety of systems ranging from biological cells to amorphous magnets. The present study would add to the list, having examined plateau vertexes from a classical fluid point of view.

The models emulate fluid structure in several respects. First, the number of significant oscillations in $g(r)$ decreases with decreasing number density. In so doing, the signatures of two phases, liquid and gas, are apparent. For the experimental run illustrated, liquidlike features were most prominent when ρ exceeded 30 particles/cm^2; gaslike morphology was most evident

for lower density samples. This interpretation follows simply from comparing the Figure 6 data with the $g(r)$ of Figure 2. Note that successions of data offer novel, modelistic views of liquid → gas transitions.

Phase properties are also realized in density plots such as in Figure 7. One sees how a liquid morphology (top panel) demonstrates a nested shell structure about the reference particle. Such a structure is lacking in gaslike states (lower panel), the shells having been "smeared" over many degrees of freedom. Equation 5 accents this point by approximating the number of particles in the first coordination sphere. Not surprisingly given the nature of plateau vertexes, this number is ca. 3 for the samples evincing liquid characteristics. Note that the analogies with real liquids and gases should not be pushed beyond proper bounds. For example, in the model systems, there is no transition heat and/or involvement of interfaces during changes from liquid to gas.

In a second respect, the data mimic fluids via the u functions. Clearly, a repulsive component or wall is most prominent in the u functionality at low r. The attractive component, or well portion, extends up to a few nearest neighbor separation lengths for the highest density samples and less than two lengths for lower density cases. An analogous situation holds for potentials in atomic fluids, as depicted in Figure 2. Interestingly, the u can be used to generate close facsimiles of experimental $g(r)$ by Monte Carlo calculations. This means two important things. One is that a major assumption seems justified, namely that a foam sample, at any given instant can be regarded as a pseudoequilibrium structure. Second, eq 4 offers a concise bridge between the potential and the correlation functions. There appears little need to apply higher orders of the BYG hierarchy.

As with all models, one must be cognizant of the illusions. For example, there is no true repulsive force between the foam vertexes. Rather, repulsion mimicry derives from the cohesive forces operating among the surfactant and water molecules composing each vertex. An analogous situation holds for colloidal particles dispersed in a liquid. Since no two vertexes can occupy the same region of space simultaneously (due to repulsive interactions between molecules), this factor contributes only to the repulsion mimicry. An anonymous reviewer has offered that because of von Neumann's law,[7] short gas bubble sides have comparatively short lifetimes. This factor leads to statistical underrepresentation of short nearest neighbor lengths; this also contributes to the repulsion mimicry.

Quantities L, Z, $S^{(2)}$, and best-fit Morse parameters contribute additional information about phase morphology and operating potentials. L can be viewed analogous to a Lindemann parameter.[28] When a fluid is near its freezing temperature, the Lindemann parameter is generally about 0.1. The L values recorded in this work exceeded this value, increasing as the gaslike states were accessed. Obviously, the data are most akin to a fluid significantly above its freezing point.

The compressibility factor Z and correlation entropy $S^{(2)}$ offer thermodynamic quantities based on the statistical structure. Notably, real fluids which are strongly interacting show a minimum in Z-versus-ρ. This is mirrored in data such as in Figure 9. In turn, the deviations from ideal gas behavior are quantified for the higher density samples. The observed functionality of $S^{(2)}$-versus-ρ is consistent with observed Z, given that $S^{(2)}$ approaches zero for gaslike states. For comparison, $S^{(2)}$ values for the highest density foam samples are close to those of liquid sodium near 800 K.[32]

For dielectric fluids, atom pair potentials are only slightly sensitive to number density. For example, the best-fit Morse parameters (ζ, eq 7) of noble gases fall in the range 6−7, regardless of number density.[33] Things are different for the models discussed here, where the potentials are markedly ρ-dependent. The models of this work thereby emulate metallic systems, where the electric charge overlap significantly affects the potentials. The best-fit ζ values allied with the model all fall in the range 2−4. The ζ values for materials such as liquid sodium ($\zeta = 3.15$) fall in this same range.[33]

VII. Summary

Detergent foam images offer A/D models for monatomic fluids. By "A", one refers to the source materials—soapsuds in plexiglass boxes—upon which all the analyses are based. By "D", the process by which the 2D images are transposed into virtual space particles of a well-defined functionality is duly recognized. Both A and D aspects are integral to the model, its tuning, and applications. Notably, model data offer the phase signatures of both liquid and gas states and the pair potentials akin to metallic systems.

The experiments are both straightforward and economical given the digital scanners and PCs of present day. Real fluids are sufficiently problematic that foam models may increase our intuition about the atomic scale.

Acknowledgment. The authors are grateful to Drs. James Glazier and Dimitri Udler for informative reprint materials and discussions about foam models. Support from the Department of Chemistry at Loyola University of Chicago and the technical assistance of J. E. Graham and Joseph Brunzelle are further appreciated. The comments and criticism of Professor Willetta Greene-Johnson and an anonymous reviewer are appreciated.

References and Notes

(1) Bragg, L.; Nye, J. F. *Proc. R. Soc. London* **1947**, *A190*, 474.

(2) See, for example, Alder, B. J.; Wainwright, T. E. *J. Chem. Phys.* **1960**, *33*, 1439. This work describes computer simulations of atomic fluids using populations of 500 particles.

(3) Dyson, J. *Proc. R. Soc.* **1949**, *199*, 130.

(4) Fukushima, E.; Ookawa, A. *J. Phys. Soc. Jpn.* **1953**, *8*, 280, 609; *9*, 44, *10*, 970, 139.

(5) See, for example: Smith, C. S. Grain Shapes and Other Metallurgical Applications of Topology. In *Metal Interfaces*; American Society for Metals: Cleveland, 1952; p 65.

(6) Bernal, J. D. *Nature (London)* **1959**, *183*, 141; **1960**, *185*, 68; *Proc. R. Soc. London* **1964**, *280*, 299.

(7) Glazier, J. A.; Gross, S. P.; Stavans, J. *Phys. Rev. A* **1987**, *36*, 306. Stavans, J.; Glazier, J. A. *Phys. Rev. Lett.* **1989**, *62*, 1318.

(8) Representative studies which model the structure and dynamics of cellular materials (especially foams) can be found in: Srolovitz, D. J.; Anderson, M. P.; Sahni, P. S.; Grest, G. S. *Phys. Rev. Lett.* **1983**, *50*, 263. Weaire, D.; Kermode, J. P. *Philos. Mag. B* **1984**, *50*, 379. Wejchert, J.; Weaire, D.; Kermode, J. P. *Philos. Mag. B* **1986**, *53*, 15. Beenakker, C. W. J. *Phys. Rev. Lett.* **1986**, *57*, 2454; Beenakker, C. W. J. *Phys. Rev. A* **1988**, *37*, 1697. Fradkov, V. E.; Magnasco, M. O.; Udler, D.; Weaire, D. *Philos. Mag. Lett.* **1993**, *67*, 203. Kawasaki, K.; Nagai, T.; Nakashima, K. *Philos. Mag. B* **1989**, *60*, 399. Magnasco, M. O. *Philos. Mag. B* **1992**, *65*, 895. Magnasco, M. O. *Philos. Mag. B* **1994**, *69*, 397. Rivier, N. *Philos. Mag. B* **1983**, *47*, L45. Flyvbjerg, H. *Phys. Rev. E* **1993**, *47*, 4037.

(9) Weaire, D.; Rivier, N. *Contemp. Phys.* **1984**, *25*, 49. Stavans, J. *Rep. Prog. Phys.* **1993**, *56*, 733; Glazier, J. A.; Weaire, D. *J. Phys.: Condens. Matter* **1992**, *4*, 1867. Glazier, J. A. Dynamics of Cellular Patterns, Dissertation, University of Chicago, 1989.

(10) See, for example, Levitan, B.; Slepyan, E.; Krichevsky, O.; Stavans, J.; Domany, E. *Phys. Rev. Lett.* **1994**, *73*, 756. de Icaza, M.; Jimenez-Ceniceros, A.; Castano, V. M. *J. Appl. Phys.* **1994**, *76*, 7317. Krichevsky, O.; Stavans, J. *Phys. Rev. B* **1993**, *46*, 10579. Levitan, B. *Phys. Rev. Lett.* **1994**, *72*, 4057.

(11) Stine, K. J.; Rauseo, S. A.; Moore, B. G.; Wise, J. A.; Knobler, C. M. *Phys. Rev. A* **1990**, *41*, 6884. Berge, B.; Simon, A. J.; Libchaber, A. *Phys. Rev. A* **1990**, *41*, 6893.

(12) Mohwald, H. *Annu. Rev. Phys. Chem.* **1990**, *41*, 441.

(13) McConnell, H. M. *Annu. Rev. Phys. Chem.* **1991**, *42*, 171.

(14) Knobler, C. M. *Annu. Rev. Phys. Chem.* **1992**, *43*, 207. Knobler, C. M. *Adv. Chem. Phys.* **1990**, *77*, 397.

(15) See, for example: Graham, D. J. *J. Phys. Chem.* **1991**, *95*, 993. Graham, D. J.; LaBrake, D. L. *J. Phys. Chem.* **1991**, *95*, 997. Graham, D. J.; LaBrake, D. L. *J. Phys. Chem.* **1993**, *97*, 5594. Graham, D. J.; LaBrake, D. L. *Appl. Spectrosc.* **1993**, *47*, 625. Graham, D. J.; Magdalinos, P.; Tosi, M. *J. Phys. Chem.* **1995**, *99*, 4757.

(16) Graham, D. J.; Magdalinos, P.; Pimentel, D. *J. Phys. Chem. B.* **1997**, *101*, 11212.

(17) Graham, D. J. In preparation.

(18) Adamson, A. W. *Physical Chemistry of Surfaces*, 4th ed.; Wiley: New York, 1982.

(19) Altmann, S. L. *Icons and Symmetries*, Clarendon: Oxford, 1992.

(20) Barker, J. A.; Henderson, D. *Rev. Mod. Phys.* **1976**, *48*, 587. Egelstaff, P. A. *An Introduction to the Liquid State*; Academic: New York, 1967. Hansen, J. P.; McDonald, I. R. *Theory of Simple Liquids*; Academic: London, 1976.

(21) Blum, L.; Narten, A. H. *Adv. Chem. Phys.* **1976**, 203. Gingrich, N. S. *Rev. Mod. Phys.* **1943**, *15*, 90.

(22) See, for example: Nowick, A. S.; Mader, S. R. *IBM J.* **1965**, *Sept.-Nov.*, 358.

(23) Hill, T. L. *Introduction to Statistical Thermodynamics*; Dover: New York, 1986; Chapter 17.

(24) See, for example: Berstein, R. B.; Muckerman, J. T. *Adv. Chem. Phys.* **1967**, *12*, 389.

(25) See, for example: Andersen, H. C.; Chandler, D.; Weeks, J. D. *Adv. Chem. Phys.* **1976**, 105.

(26) Hill, T. L. *Statistical Mechanics*; McGraw-Hill: New York, 1956; Chapter 6.

(27) Braun, J.; Abney, J. R.; Owicki, J. C. *Nature* **1984**, *310*, 316.

(28) Goodstein, D. L. *States of Matter*; Dover: New York, 1985; Chapter 4.

(29) See, for example: Wheatley, P. J. *The Determination of Molecular Structure*; Dover: New York, 1968; Chapter 8.

(30) Wallace, D. C. *Phys. Lett. A* **1987**, *122*, 418.

(31) Prud'homme, R. K.; Khan, S. A. *Foams: Theory, Measurements, and Applications*; Dekker: New York, 1996. Laradji, M.; Guo, H.; Grant, M.; Zuckermann, M. J. *Adv. Chem. Phys.* **1995**, *89*, 159.

(32) Waseda, Y. *The Structure of Non-Crystalline Materials*; McGraw-Hill: New York, 1980.

(33) Doye, J. P. K.; Wales, D. J. *Science* **1996**, *271*, 484.